In Vivo Selection Yields AAV-B1 Capsid for Central Nervous System and Muscle Gene Therapy

Sourav R Choudhury[1,2], Zachary Fitzpatrick[3], Anne F Harris[1,2], Stacy A Maitland[1,2], Jennifer S Ferreira[1,2], Yuanfan Zhang[4], Shan Ma[2,5], Rohit B Sharma[6], Heather L Gray-Edwards[7], Jacob A Johnson[8], Aime K Johnson[8], Laura C Alonso[6], Claudio Punzo[2,5], Kathryn R Wagner[4], Casey A Maguire[3], Robert M Kotin[2,9], Douglas R Martin[7,10] and Miguel Sena-Esteves[1,2]

[1]Department of Neurology, University of Massachusetts Medical School, Worcester, Massachusetts, USA; [2]Gene Therapy Center, University of Massachusetts Medical School, Worcester, Massachusetts, USA; [3]Department of Neurology, Massachusetts General Hospital and Program in Neuroscience, Harvard Medical School, Boston, Massachusetts, USA; [4]The Hugo W. Moser Research Institute, Kennedy Krieger Institute and Departments of Neurology and Neuroscience, Johns Hopkins School of Medicine, Baltimore, Maryland, USA; [5]Department of Ophthalmology, University of Massachusetts Medical School, Worcester, Massachusetts, USA; [6]Diabetes Center of Excellence, University of Massachusetts Medical School, Worcester, Massachusetts, USA; [7]Scott-Ritchey Research Center, College of Veterinary Medicine, Auburn University, Auburn, Alabama, USA; [8]Department of Clinical Sciences, College of Veterinary Medicine, Auburn University, Auburn, Alabama, USA; [9]Voyager Therapeutics, Cambridge, Massachusetts, USA; [10]Department of Anatomy, Physiology & Pharmacology, College of Veterinary Medicine, Auburn University, Auburn, Alabama, USA

Adeno-associated viral (AAV) vectors have shown promise as a platform for gene therapy of neurological disorders. Achieving global gene delivery to the central nervous system (CNS) is key for development of effective therapies for many of these diseases. Here we report the isolation of a novel CNS tropic AAV capsid, AAV-B1, after a single round of *in vivo* selection from an AAV capsid library. Systemic injection of AAV-B1 vector in adult mice and cat resulted in widespread gene transfer throughout the CNS with transduction of multiple neuronal subpopulations. In addition, AAV-B1 transduces muscle, β-cells, pulmonary alveoli, and retinal vasculature at high efficiency. This vector is more efficient than AAV9 for gene delivery to mouse brain, spinal cord, muscle, pancreas, and lung. Together with reduced sensitivity to neutralization by antibodies in pooled human sera, the broad transduction profile of AAV-B1 represents an important improvement over AAV9 for CNS gene therapy.

Received 11 November 2015; accepted 12 April 2016; advance online publication 7 June 2016. doi:10.1038/mt.2016.84

INTRODUCTION

Adeno-associated viral vectors have emerged as one of the preferred delivery agents for clinical gene therapy. In 2012, Glybera, an adeno-associated virus (AAV)-1 vector encoding lipoprotein lipase, became the first gene therapy product to receive marketing approval in the European Union.[1] Other clinical trials using AAV vectors have yielded positive outcomes.[2–4] Several clinical trials for neurological disorders have shown excellent safety profiles, but therapeutic impact has been relatively modest.[5–10] A majority of these central nervous system (CNS) trials involve direct injection of AAV vectors into the brain parenchyma. While this approach has been successful for gene transfer to a localized structure of the CNS, most neurodegenerative disorders exhibit cell loss in multiple structures, including amyotrophic lateral sclerosis, frontotemporal dementia, Rett syndrome, and Huntington's disease, among others. Achieving efficient widespread neuronal gene transfer is therefore crucial for the development of effective new therapies for a majority of neurological diseases.

Systemic administration of AAV9 through the vasculature mediates widespread gene transfer in the neonatal CNS.[11,12] The blood–brain barrier is however fully formed by adulthood and poses the greatest obstacle to successful transduction of adult CNS by systemic AAV delivery. AAV9 was the first capsid shown to cross the BBB in both neonate and adult animals after intravascular infusion,[12] and has become the standard for systemic AAV-mediated CNS gene therapy.[13–19] However, the neuronal transduction of AAV9 in adult animals after systemic administration is scant,[12,20] except in spinal cord motor neurons,[12,21,22] as well as neurons in the dorsal root ganglia,[21] and enteric nervous system.[23,24] The resulting therapeutic consequence is illustrated by the decrease in motor neuron transduction and accompanying decline in phenotypic rescue with age of treatment by intravascular administration of an AAV9-SMN vector in spinal muscular atrophy mice.[13] There is therefore a need for novel AAV vectors capable of greater neuronal gene transfer in the adult brain after systemic delivery.

The AAV virion consists of a nonenveloped icosahedral capsid, comprised of 60 subunits of VP1, VP2, and VP3 capsid proteins in a ratio of ~1:1:10, and an encapsidated single-stranded DNA viral genome. In addition to protecting the genome, the capsid mediates interactions with cell surface receptors and postentry intracellular trafficking and as such, is the major determinant of tropism. The biodistribution of AAV depends largely on the amino acid sequence of nine surface exposed loops (variable region, VR-I to -IX) in VP3, which vary across capsids.[25,26] The cell-surface receptors used by AAV to interact with host cells are known for some capsids,[27–30] but the knowledge remains incomplete on all structural determinants responsible for AAV tropism. The majority of AAV capsids

Correspondence: Correspondence should be addressed to M.S.-E. (miguel.esteves@umassmed.edu) Miguel Sena-Esteves, Gene Therapy Center, University of Massachusetts Medical School 368 Plantation Street, ASC6-2055, Worcester, Massachusetts 01605, USA. E-mail: miguel.esteves@umassmed.edu

currently being used in research and in clinical trials are natural variants isolated from non-human primate and human tissues.[31–33] Capsids of these natural isolates can be engineered to generate novel AAV capsids with enhanced properties.[34] Directed molecular evolution is a high-throughput method used to generate new AAV capsids capable of transducing target cell populations.[35–37] The process of directed evolution simulates that of natural evolution, where selective pressure yields genetic variants with specific biological properties. In contrast to natural evolution, large pools of genetic variants are present simultaneously in directed evolution, thus compressing the time of selection from geologic timescales to a matter of weeks or months. Unlike other capsid modification methods based on rational design (*e.g.*, peptide grafting, receptor targeting, or detargeting), directed evolution or library screening does not require prior knowledge of molecular events involved in the selection process. A caveat of *in vitro* directed evolution of AAV is that it cannot simulate complex biological events, such as crossing blood–organ barriers after vascular infusion where capsids encounter a myriad of serum proteins and small molecules as well as the fluid dynamics of blood flow. A few studies have succeeded in selecting new capsids by *in vivo* biopanning of AAV capsid libraries. These include synthetic capsids capable of targeting cardiomyocytes,[38] crossing the seizure-compromised blood–brain barrier,[39] transducing photoreceptors from the vitreous humor,[40] or targeting xenotransplanted human hepatocytes.[41] Recently, two re-engineered capsids, AAV-AS[42] and AAV-PHP.B[43] were shown to be superior to AAV9 for systemic gene delivery to the CNS and capable of high efficiency neuronal transduction. Here, we used *in vivo* selection to isolate new AAV capsids effective for CNS gene transfer.

RESULTS

Single round of selection in mouse yields novel synthetic capsids

We sought to isolate chimeric AAV variants capable of CNS transduction upon systemic delivery in adult mice after one round of library selection (**Figure 1a**). We constructed an AAV capsid library by DNA shuffling of AAV1, 2, 4, 5, 6, 8, 9, rh8, rh10, rh39, and AAVrh43 capsid genes. The parental capsids were chosen for their ability to transduce CNS upon intravenous delivery in neonatal mice.[11] The plasmid library had a maximum diversity of 2×10^7 capsids, based on transformation efficiency. Sanger sequencing of individual capsids from the viral library confirmed the chimeric nature of capsid genes in the library (**Supplementary Figure S1**). The AAV library was infused into adult C57BL/6 mice via the tail vein at 1×10^{11} or 5×10^{11} genome copies, and tissue resident capsid genes were polymerase chain reaction (PCR) amplified from brain and liver after 3 days. Of capsids isolated from brain, AAV-B1 was the only one amplified from the mouse infused at the lower dose, while AAV-B2, B3, and B4 were isolated from the high dose. In contrast, numerous

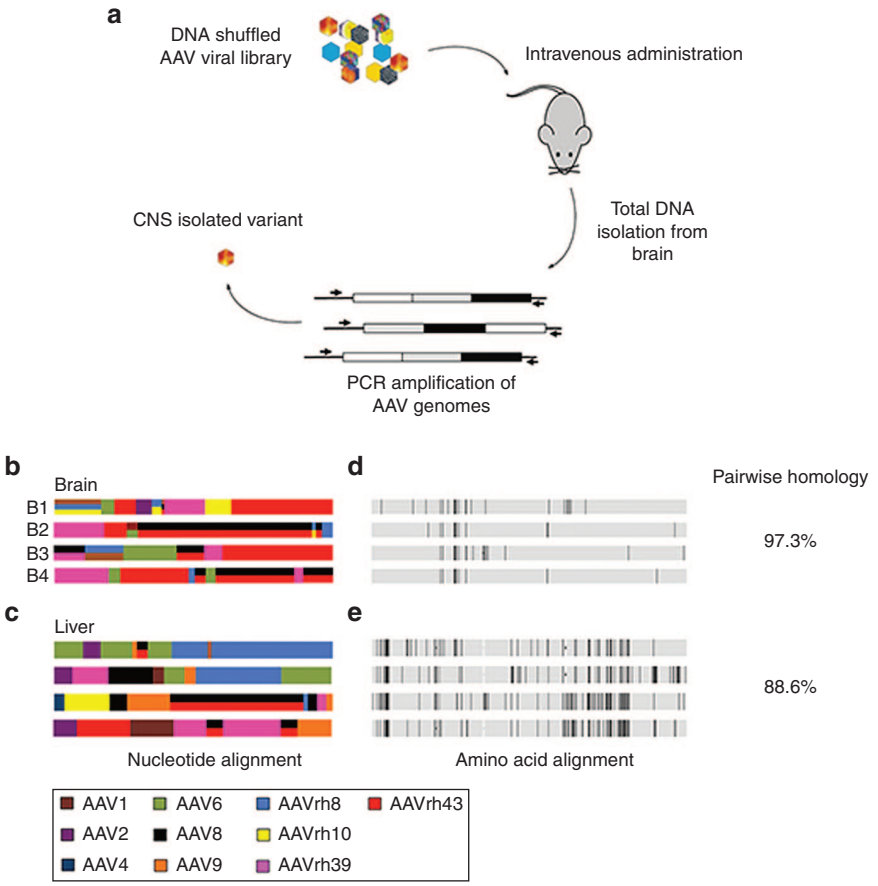

Figure 1 Single round *in vivo* biopanning. (**a**) Selection strategy. (**b,c**). Parental capsid gene contribution to new chimeric capsid genes isolated from (**b**) brain (AAV-B1, -B2, -B3, and -B4) and (**c**) liver. (**d,e**) Amino acid homology among capsids isolated from (**d**) brain and (**e**) liver. Gray areas indicate homology; black lines indicate nonhomologous amino acids. % homology is calculated for amino acid composition.

capsids were found in liver of mice infused at either dose, the major depot organ of systemically infused AAV. All new AAV capsid genes were chimeric, but the VP3 capsid genes of brain clones (AAV-B1 through B4) were mostly comprised of DNA derived from either AAV8 or AAVrh43 (**Figure 1b**), while liver-isolated capsid genes were more diverse (**Figure 1c**). Analysis of capsid protein sequences revealed greater homology between capsids isolated from brain (97.3% pairwise homology) (**Figure 1d**) compared to capsids isolated from liver (88.6% pairwise homology) (**Figure 1e**).

Brain-selected AAV-B1 transduces mouse neuronal populations, and is superior to AAV9 for CNS gene transfer

The CNS transduction profile of AAV-B1 was assessed after systemic delivery in adult mice using a green fluorescent protein (GFP) expression cassette (**Figure 2a**). AAV-B1 vector transduced neuronal, glial and endothelial populations throughout the CNS (**Figure 2b**, **Supplementary Figures S2 and S3**). Neuronal transduction was apparent in multiple regions of the cerebral cortex (**Supplementary Figure S3a**), including the primary (**Figure 2b**)

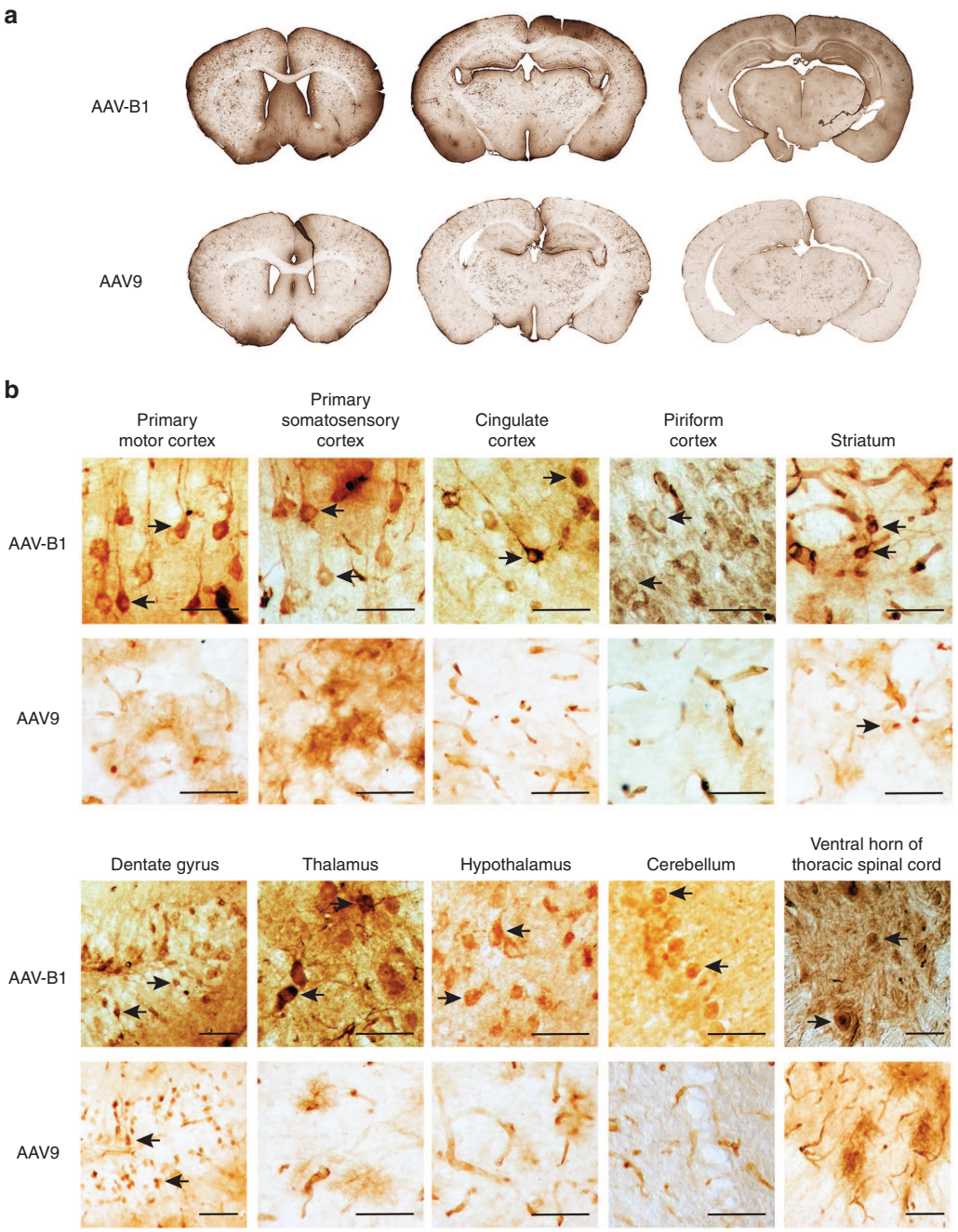

Figure 2 Central nervous system (CNS) transduction profile of AAV-B1 vector after intravascular infusion in adult mice. (**a**) Overview of green fluorescent protein (GFP) distribution in brains of AAV-B1- and AAV9-injected mice (2×10^{12} vg/mouse). Representative images of coronal brain sections located at +0.5, –1.80, and –3.00 mm (left to right) in relation to bregma are shown. (**b**) Transduction of neuronal populations in different CNS regions of AAV-B1- and AAV9-injected mice. Black arrows indicate examples of GFP-positive neurons identified by morphology. Bar = 50 µm.

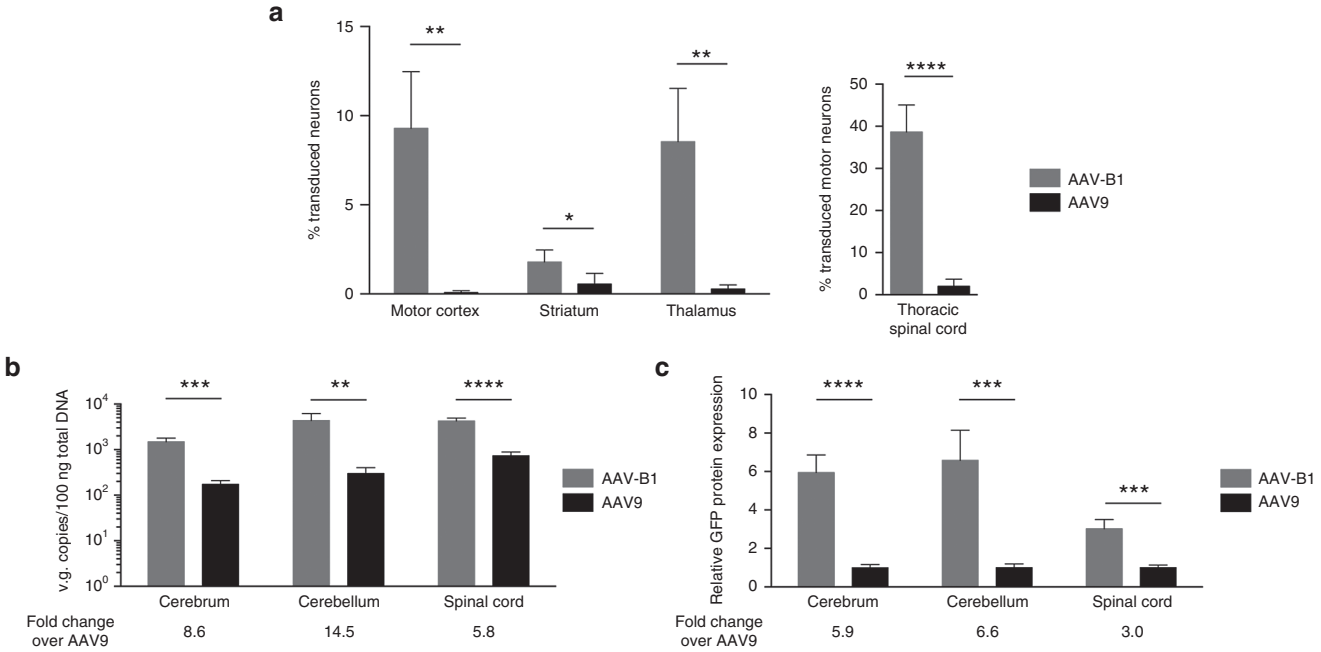

Figure 3 Quantitative assessment of AAV-B1 central nervous system transduction efficacy. (**a**) Quantification of percent green fluorescent protein (GFP)-positive neurons in motor cortex, striatum, and thalamus, and percent GFP-positive motor neurons in thoracic spinal cord of mice injected with AAV-B1-GFP or AAV9-GFP vectors. Data shown is mean ± SD ($n = 4$ biological replicates per group). (**b,c**) Comparison of (**b**) AAV vector genome content and (**c**) GFP protein expression in cerebrum, cerebellum, and spinal cord of mice injected with 5×10^{11} vg AAV-B1 or AAV9 ($N = 4$ animals per group). Age-matched noninjected mice were included as controls (not shown). Signal intensity of GFP was normalized to corresponding β-actin signal intensity for quantitative comparison. *$P < 0.05$, **$P < 0.01$, ***$P < 0.001$, ****$P < 0.0001$ by Student's two-tailed unpaired *t*-test.

and secondary (**Supplementary Figure S2**) motor and somatosensory cortices, cingulate cortex and piriform (olfactory) cortex (**Figure 2b**). The majority of cortical neurons transduced were pyramidal cells in layer III, although transduced neurons in layers V and VI were also apparent (**Supplementary Figure S3a,b**). A sparse number of DARPP32-positive medium spiny neurons in the striatum were found transduced (**Supplementary Figure S3c**). In the hippocampal formation, we found transduced granule cells in dentate gyrus (**Figure 2b**, **Supplementary Figure S3d**) and pyramidal neurons in CA1-CA3 areas (**Supplementary Figure S2**). Similar patterns of gene transfer to hippocampal neurons have been reported for AAV9.[44] Neurons in the thalamus (**Figure 2b**, **Supplementary Figure S3d**), hypothalamus, amygdala (**Figure 2b**), and tyrosine hydroxylase-positive dopaminergic neurons in the substantia nigra (**Supplementary Figure S3d**) were similarly transduced with AAV-B1. In the cerebellum, AAV-B1 vector-transduced Purkinje cells (identified by calbindin D-28K costaining) (**Figure 2b**, **Supplementary Figure S3e**) as well as neurons in the granular layer. Finally, AAV-B1 vector transduced motor neurons throughout the spinal cord (**Figure 2b**, **Supplementary Figures S2 and S3f**). In comparison, sparse neuronal transduction could be observed with dose-matched AAV9 vector (**Figure 2**, **Supplementary Figure S3**).

In addition to the neuronal tropism, AAV-B1 also transduced endothelial cells in the brain and spinal cord identified by the distinct morphology of blood vessels in CNS and confirmed by costaining for CD31 (**Supplementary Figure S3g**). AAV-B1 also transduced glial cells such as mature oligodendrocytes (identified by costaining for APC) (**Supplementary Figure S3h**) and astrocytes (identified by morphology) (**Supplementary Figure S3i**). Strong transduction of the choroid plexus was also apparent (**Supplementary Figure S2**).

AAV-B1 has higher neuronal transduction efficiency compared to AAV9 in motor cortex (9.30% ± 1.6 for AAV-B1 versus 0.09% ± 0.05 for AAV9, or 107.4-fold), thalamus (8.54% ± 1.5 versus 0.29% ± 0.11, or 29.8-fold) and in motor neurons of the spinal cord (38.6% ± 3.2 versus 2.0% ± 0.8, or 19.3-fold), while the differential in percentage of transduced neurons is more modest in the striatum (1.79% ± 0.35 versus 0.56% ± 0.30, or 3.2-fold) (**Figure 3a**). Quantitative analysis of AAV vector genomes in different regions of the CNS revealed 5.8- to 14.5-fold higher content for AAV-B1 compared to AAV9 (**Figure 3b**). GFP protein levels throughout CNS were also consistently higher for AAV-B1 compared to AAV9 (**Figure 3c**).

AAV-B1 as a global gene therapy vector

Next, we assessed the peripheral transduction profile of AAV-B1. Liver transduction by AAV-B1 was lower than AAV9 as assessed by histological examination of GFP expression (**Figure 4a**). The vector genome content of AAV-B1 liver was 3.6-fold lower than AAV9 (**Figure 4b**), while the GFP protein levels in liver were 2.2-fold lower for AAV-B1 (**Figure 4c**). AAV-B1 proved to be highly efficient in transducing skeletal muscle and heart (**Figure 4d**) where vector genome content was 10.4- to 26.6-fold and 14.4-fold higher than AAV9, respectively (**Figure 4e**). AAV-B1 also transduced several cell populations in the pancreas, including insulin-positive β-cells (26.5%) (**Figure 4f**) and exocrine cells (86.3%) (**Figure 4g**). AAV-B1 also transduced lung alveoli efficiently (**Figure 4h**). The vector genome content in pancreas and lung was 21.3- and 14.1-fold higher for AAV-B1 than AAV9, respectively (**Figure 4i,j**).

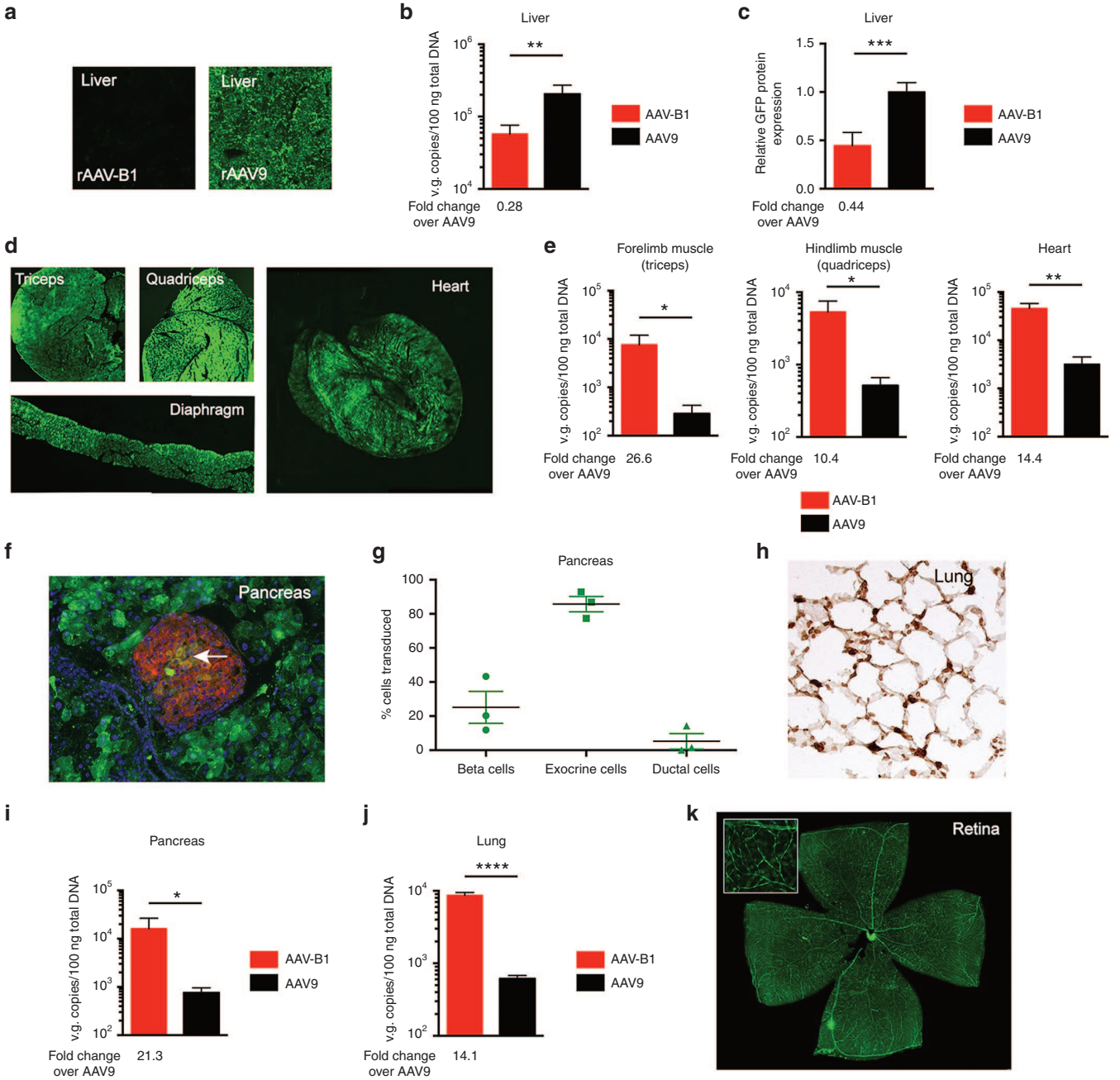

Figure 4 AAV-B1 biodistribution to other mouse tissues after intravascular delivery. Green fluorescent protein (GFP) expression in (**a**) liver of AAV-B1- and AAV9-injected mice (2×10^{12} vg/mouse), (**d**) skeletal muscle (triceps and quadriceps), diaphragm and heart, (**f**) pancreas, (**h**) lung, and (**k**) retina of AAV-B1-injected mice (5×10^{11} vg/mouse). White arrow in (**f**) indicates GFP (green)-positive insulin (red)-producing beta cells. Inset in (**k**) shows individual GFP-positive blood vessels. Comparison of AAV vector genome content in (**b**) liver, (**e**) muscle groups, (**i**) pancreas, and (**j**) lung, and GFP protein levels in (**c**) liver of mice injected with 5×10^{11} vg AAV-B1 or AAV9 is shown (N = 4 animals per group). (**g**) Quantification of percentage of GFP+ population of beta cells (identified by colocalization with insulin), exocrine cells and ductal cells (identified by morphology). *P < 0.05, **P < 0.01, ***P < 0.001, ****P < 0.0001 by Student's two-tailed unpaired t-test.

Finally, retinal endothelium was also transduced at high efficiency (Figure 4k), a property that is unique to AAV-B1 (ref. 45).

CNS tropism of mouse-selected AAV-B1 extends to a large animal species

Several novel therapies have been tested in feline models of neurological disorders prior to clinical trials.[46–49] To investigate whether the CNS tropism of mouse-selected AAV-B1 is reproducible in a large animal species relevant to translational research, we infused AAV-B1 vector systemically into a normal juvenile cat through the carotid artery. We observed relatively sparse but widespread neuronal gene transfer throughout the cat brain (Figure 5). Mirroring the neuronal transduction pattern in mouse, AAV-B1 transduced neurons in the cat cerebral cortex, striatum, hippocampus, thalamus and Purkinje neurons in the cerebellum (Figure 5a). In addition, we observed transduced motor neurons throughout

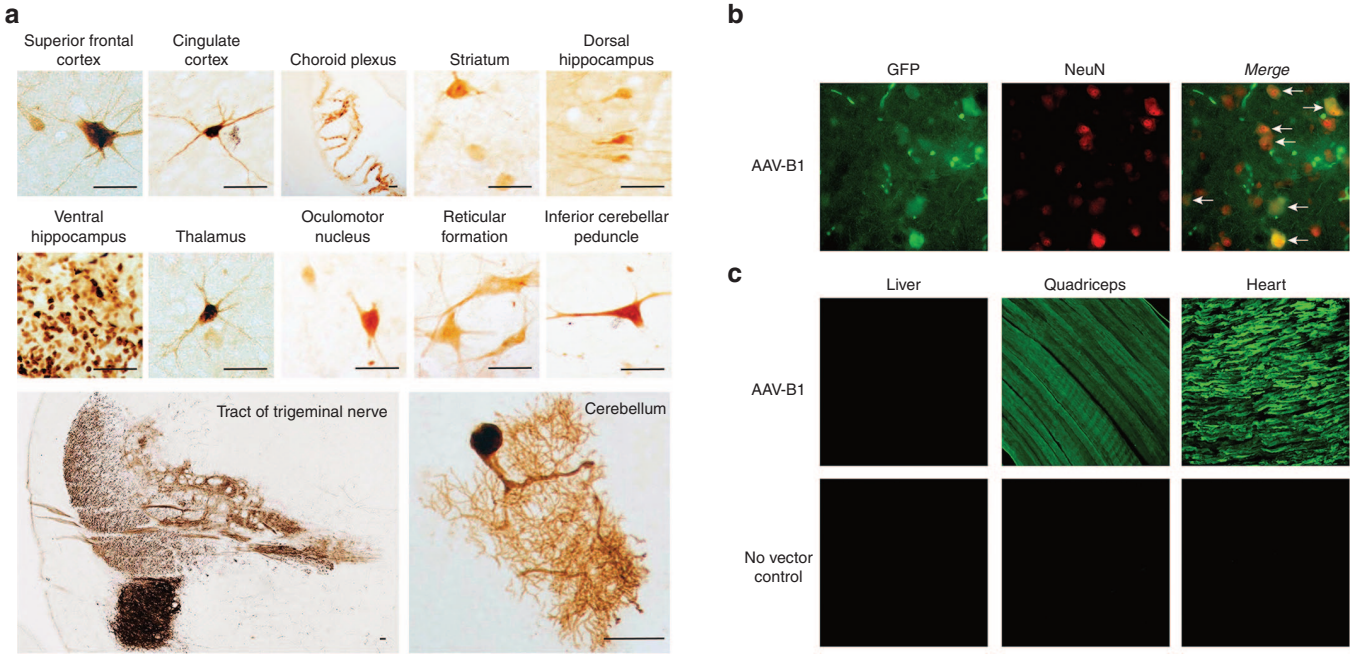

Figure 5 Neuronal transduction and biodistribution to other tissues after systemic delivery of AAV-B1 vector in cat. (**a**) Green fluorescent protein (GFP) distribution in the cat brain after systemic delivery of 3.4×10^{12} vg AAV-B1 vector. Representative images show GFP-positive cells with neuronal morphology in various structures in the brain. Image of tract of trigeminal nerve shows GFP staining of nerve fibers. Bar = 50 µm. (**b**) Transduced cells were identified by double immunofluorescence staining with antibodies to GFP and pan-neuronal marker NeuN. (**c**) GFP expression in liver, quadriceps and heart of AAV-B1 injected cat. Age matched noninjected cat was included as control.

the midbrain. The neuronal identity of transduced cells was confirmed by co-staining with a neuronal marker (Figure 5b). Unlike in mouse, we found no indication that AAV-B1 transduced endothelial cells in the cat CNS. Paralleling observations in mouse, negligible transduction of cat liver was observed with AAV-B1, while strong gene transfer to skeletal and cardiac muscle could be detected (Figure 5c).

Biophysical characteristics of AAV-B1

AAV-B1 differs from AAV8, its closest parental capsid, by 19 amino acids (A24D, Q84K, A98V, L129F, P148Q, R152E, T157S, S223N, L235M, A268S, Q412E, T414S, T416Q, T452S, N458R, T461Q, G463L, G467A, and F502S) (**Supplementary Figure S4**). Structural modeling of AAV-B1 capsid based on the AAV8 template showed that most amino acids in VP3 that differ between the two capsids cluster in two regions, the βG strand (Q412E, T414S, T416Q) and the VR-IV loop (T452S, T461Q, G463L, and G467A) that were apparently derived from the AAVrh10 *cap* gene. The A268S substitution in the VR-I loop is a small side chain residue in representative AAV serotypes and is considered a conservative change. All surface exposed residues in VR-IV were of AAVrh10 origin except for N458R, which is not identified with any representative AAV genotypes (Figure 6a,b). Despite the high degree of homology between AAV-B1 and AAV8, we confirmed that AAV-B1 and AAV8 have distinct biodistribution profiles after systemic infusion in adult mice (**Supplementary Figure S5**).

Pre-existing humoral immunity is a major challenge for AAV-based clinical gene therapy.[50] We used a pooled human immunoglobulin-G (IVIG) neutralization assay to assess the ability of AAV-B1 to transduce cells in the presence of anti-AAV antibodies. We found AAV-B1 to be modestly, yet significantly more resistant to neutralization than AAV9 at all concentrations tested (Figure 6c, **Supplementary Figure S6**).

To determine whether AAV-B1 uses the same cell-surface receptor as AAV9 given the shared CNS and muscle tropism, we performed cell binding assays using parental (Pro5) and sialic acid-deficient (Lec2) Chinese hamster ovary (CHO) cells. Surface exposed sialic acid residues allow for binding of capsids such as AAV1 (ref. 27), AAV4 (ref. 28), AAV5 (ref. 28), and AAV6 (ref. 27) to Pro5 cells, while surface glycans on Lec2 cells are nonsialylated and thus have exposed galactose residues used by AAV9 as a receptor.[29,30] AAV-B1 did not exhibit preferential binding to either cell line, indicating that neither terminal sialic acid nor terminal galactose preferentially act as primary glycan receptors for AAV-B1 capsid (Figure 6d).

DISCUSSION

Treatment of diffuse and multifocal neurological pathologies by direct intraparenchymal injection is unlikely to lead to even distribution of the therapeutic molecule in the CNS, even with the use of advanced infusion techniques such as convection enhanced delivery,[51] or by injection into axonally connected structures.[52–55] In contrast, a single systemic infusion of AAV-B1 can mediate gene transfer to neuronal populations in multiple structures throughout the CNS, making it an attractive candidate for development of AAV-based gene therapies for neurological disorders. AAV-B1 is demonstrably superior to AAV9 for CNS transduction (approximately one log higher). Our observation that intravascular delivery of 1×10^{14} vg/kg AAV9 vector resulted in transduction of <10% of spinal cord motor neurons, is supported by some

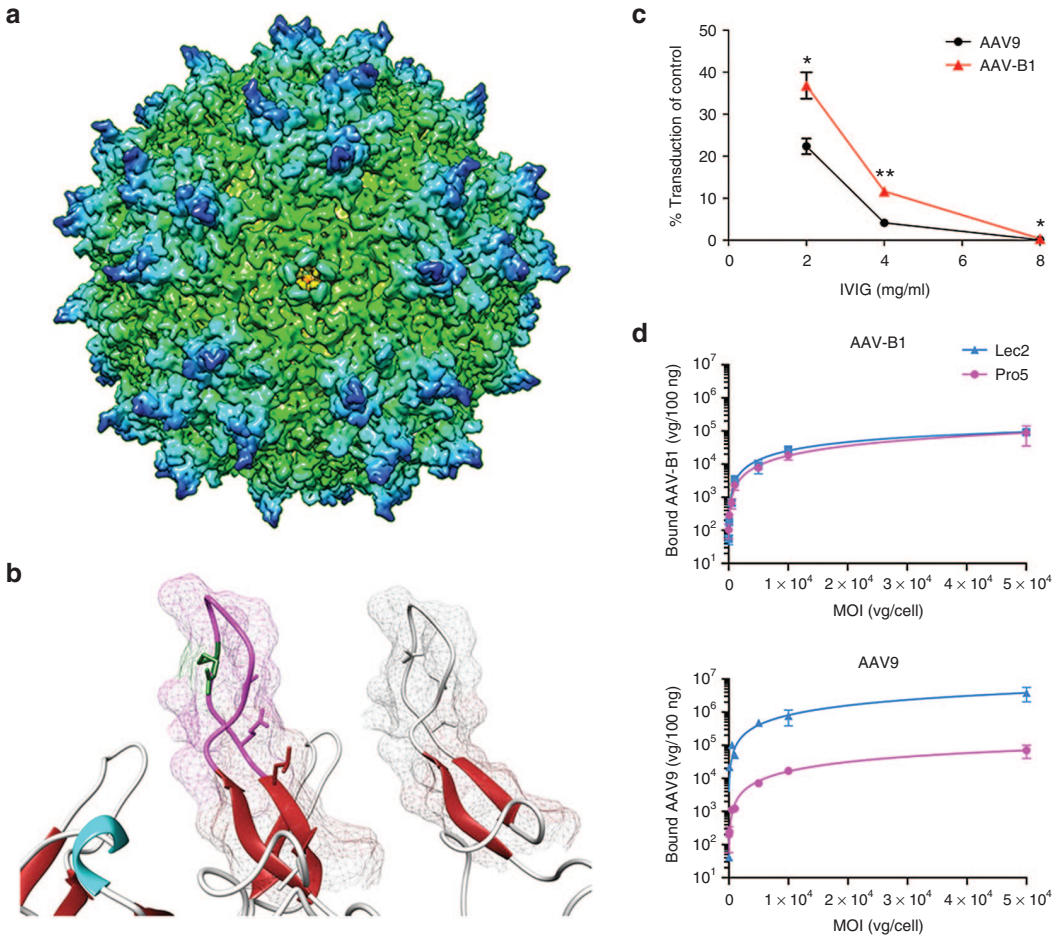

Figure 6 Structure, binding, and neutralizing antibody analysis of AAV-B1. (**a**) Predicted molecular model of AAV-B1 capsid. (**b**) Surface exposed variable region-IV (VR-IV) of AAV-B1 (left) and AAV8 (right). (**c**) Pooled human immunoglobulin-G neutralization assay and (**d**) CHO cell binding assay of AAV-B1 and AAV9 vectors. Data shown as mean ± standard error of the mean in (**c**), and as mean ± SD in (**d**). Experiment was performed with $N = 3$ biological replicates. $^*P < 0.05$ by one-way analysis of variance.

reports,[12,14] but is considerably lower than other estimates.[21] One possible reason of such discrepancy could be that GFP expression from the weak intron-less CBA promoter is below the detection limit of our immunohistochemical (IHC) method. Another important characteristic of AAV-B1 is the consistency of pan-neuronal transduction in both mouse and cat brain, as numerous naturally occurring models of neurodegenerative diseases in the latter intermediate size species are often used in the translation of proof-of-concept experiments in mice to clinical trials in humans. It is important to cautiously note here however that data from cats need not translate to larger species such as non-human primates and ultimately humans. Further, a dose of 1×10^{14} vg/kg corresponds to 6.5×10^{15} vg for a 65 kg adult human, an onerous scale of production with current technology of GMP-compliant AAV production.

In addition to being extremely potent for CNS gene transfer as expected from the screening strategy of this study, AAV-B1 is also highly effective for gene transfer to a number of peripheral tissues including skeletal muscle, heart, and lung. The broad transduction profile of AAV-B1 suggests several gene therapy applications, including those for systemic correction of monogenic neurometabolic disorders, muscular dystrophies and diabetes, as well as disorders involving the alveolar epithelium such as surfactant deficiencies. One such potential therapy application is for Pompe disease, a lysosomal storage disease that manifests as muscular atrophy, cardiorespiratory failure and glycogen storage in motor neurons.[56] AAV9 has limited therapeutic effect in adult Pompe disease mice,[57] possibly due to inefficient mannose-6-phosphate receptor-mediated enzyme uptake in skeletal muscle[58] and insufficient AAV9 gene transfer efficiency. In addition, the unique retinal vasculature transduction profile of AAV-B1 may be useful for gene therapy of ocular vascular disorders like diabetic retinopathy and wet age-related macular degeneration. The higher resistance of AAV-B1 to pre-existing neutralizing antibodies in pooled human sera suggests that systemic gene therapies based on this new capsid may be applicable to a broader population of patients. However, in the future, a more extensive profiling of the AAV-B1 capsid using individual patient sera, lower gc/cell of vector, and a more sensitive reporter such as firefly luciferase should be performed to more accurately determine the prevalence of AAV-B1 neutralizing antibodies in humans.

The isolation of AAV-B1 is the first instance where an AAV capsid capable of crossing a noncompromised blood–brain barrier

(BBB) has been selected from a chimeric capsid library. While the AAV-B1 capsid was selected at the lower library dose, it does not exclude the possibility of stochastic selection. This could theoretically be resolved by repeating the selection to isolate the same or homologous capsid variants. An argument against AAV-B1 being selected stochastically, however, is the greater VP3 protein homology between brain-selected capsids compared to liver-resident variants, which suggests a structure-function relationship. One or more of the amino acid differences in surface-exposed domains of AAV-B1 and AAV8 likely account for the difference in tropism between these highly homologous capsids, although the present lack of structural data for AAV VP1 and VP2 N-terminal regions[25,26] makes it difficult to speculate about the contribution of the numerous amino acid differences found in those regions to overall tropism. At the cell entry level, AAV-B1 appears to use neither sialic acid nor galactose preferentially as its cell surface receptor, similar to AAV8 whose primary receptor remains unknown. Recently, an essential receptor for AAV infection, AAVR (type I transmembrane protein, KIAA0319L) was identified.[59] AAVR serves as a critical receptor for infection of all tested serotypes, including AAV8, and thus it is likely that AAV-B1 infection would depend on AAVR. Protocols for purification of AAV-B1 for clinical purposes can be established by generating immunoligands based on camelid-derived single-domain antibody fragments (as are commercially available for AAV9 affinity matrix purification) by llama-derived phage display library screening, or by currently established anion exchange chromatography-based GMP-compliant method to prepare clinical grade AAV8 vectors.[60] Further biophysical studies for this capsid may shed light on the unique biological properties of AAV-B1.

In conclusion, AAV-B1 is a novel capsid for CNS as well as global gene therapy, with potential for clinical development.

MATERIALS AND METHODS

Library construction. PCR-based DNA shuffling was performed similar to a previously described protocol.[61] Capsid open reading frames from AAV1, 2, 4, 5, 6, 8, 9, rh8, rh10, rh39, and AAVrh43 were PCR amplified with primers designed to insert unique *Hind*III and *Xba*I sites at the 5' and 3' end of *cap* gene, respectively, cloned into an universal vector (Zero Blunt TOPO, Life Technologies, Grand Island, NY) and digested with *Hind*III and *Xba*I. Equimolar amounts of the resulting digested *cap* fragments were mixed together and fragmented with DNase I (Roche Diagnostics, Mannheim, Germany). Fragments less than 500 bp in length were gel purified and assembled by cycling 250 ng of purified DNA using *Taq* polymerase (Platinum *Taq* DNA Polymerase High Fidelity, Thermo Scientific, Rockford, IL). Cycling conditions were as follows: 94 °C, 5 minutes; 35 cycles of (94 °C, 30 seconds; slow ramping from 65 to 41 °C over 10 minutes; 72 °C, 4 minutes); 72 °C, 7 minutes. Chimeric cap genes were amplified from assembled DNA (Extensor Long Range PCR Enzyme, Thermo Scientific), digested with *Hind*III and *Xba*I and subcloned into pSub201 packaging plasmid digested with the same restriction enzymes. Shuffled plasmid library was generated by transformation of the subcloned library into high efficiency bacterial cells (MegaX DH10B T1 electrocompetent cells, Thermo Scientific), followed by isolation of plasmid DNA. Maximum theoretical diversity of plasmid library was calculated based on colony counts obtained from representative aliquot of bacteria transformed with plasmid library.

Packaging of the viral library was done as previously described.[35] Briefly, HEK293T cells grown in 150 mm dishes were transfected with 4 ng shuffled plasmid library and 25 µg each of pBluescript and pFΔ6 adenoviral helper plasmid using HEPES-buffered saline/calcium chloride cotransfection method. Seventy-two hours after transfection, cells were harvested and viral library was purified by iodixanol-gradient ultracentrifugation,[62] 100 kDa molecular weight cutoff concentration and dialysis in 1× phosphate buffer saline (PBS). DNase-resistant vector genome titer was determined by quantitative PCR (qPCR). Details of virus purification and titration are provided in a subsequent section.

In vivo *library selection.* 1×10^{11} or 5×10^{11} vector genomes of viral library were infused into adult 6–8-week-old male C57BL/6J mice through intravenous route (tail vein) (N = 1). Three days after infusion, mice were euthanized, and brain and liver harvested. Total DNA were isolated using DNeasy Blood and Tissue kit (Qiagen, Hilden, Germany) and tissue-resident capsid genes were amplified by nested PCR using primers designed to bind to 5' and 3' ends of *cap* region. Nucleotide and amino acid alignment and homology quantification were performed using Geneious (Biomatters, Auckland, New Zealand).

Vector particle production and titer quantification. The self-complementary AAV-CBA-GFP vector used in these studies carries an expression cassette comprised of the CBA promoter without an intron to drive expression of GFP and a rabbit β-globin poly-adenylation signal.

To generate AAV vectors, HEK293T cells were cotransfected with the following mix of plasmids using the calcium phosphate precipitation method: 7.96 µg transgene plasmid, 25.6 µg adenoviral helper plasmid pFΔ6, 12.2 µg AAV-B1 or AAV9 *rep-cap* packaging plasmid, per 2.1×10^{7} cells plated. Seventy-two hours post-transfection, cells were harvested and cell lysates prepared by three cycles of freeze-thawing and treated with Benzonase (Sigma-Aldrich, St. Louis, MO) (50 U/ml cell lysate, 37 °C, 30 minutes). AAV was purified from cell lysates by iodixanol density-gradient ultracentrifugation (Optiprep density-gradient medium, Axis-Shield, Oslo, Norway). Residual iodixanol was removed by replacing with Buffer B (20 mmol/l TRIS, 0.5 mol/l NaCl, pH 8.5) using a 100 kDa molecular weight cutoff centrifugation device (Amicon Ultra-15, Merck Millipore, Cork, Ireland) by three rounds of centrifugation at 1,500× g and dialyzed twice using a 10,000 molecular weight cutoff dialysis cassette (Slide-A-Lyzer, Thermo Scientific, Rockford, IL) against a 1,000-fold volume of#8232;PBS for >2 hours and once overnight at 4 °C. After treatment of stocks with DNase I (Roche Diagnostics GmbH, Mannheim, Germany, 2 U/µl vector, 37 °C, 30 minutes), the titer of AAV vectors was determined by real-time quantitative PCR (qPCR) using probe and primers specific for the rabbit β-globin polyA sequence (Integrated DNA Technologies, Coralville, IA).

Vector administration and tissue processing. The Institutional Animal Care and Use Committees at the University of Massachusetts Medical School and Auburn University reviewed and approved all experiments in mice and cats, respectively, in compliance with guidelines from the National Institutes of Health.

AAV vectors were administered via the tail vein in a volume of 200 µl into 6–8-week-old male C57BL/6J mice (Jackson Laboratory, Bar Harbor, ME). A dose of either 5×10^{11} or 2×10^{12} vector genomes (vg)/mouse was administered for immunochemical studies, while a dose of 5×10^{11} vg/mouse was administered for biodistribution analysis.

For immunochemical studies of CNS and GFP fluorescence studies of liver, mice injected at a dose of 2×10^{12} vg/mouse were trans-cardially perfused at 4 weeks postinjection first with ice cold 1× PBS, followed by 4% paraformaldehyde solution (Fisher Scientific, Fair Lawn, NJ). Tissues were harvested and postfixed in 4% paraformaldehyde solution at 4 °C for an additional 24 hours. Postfixed tissues were transferred to 30% sucrose in 1× PBS for cryoprotection. Tissues were embedded in Tissue-Tek O.C.T. compound (Sakura Finetek, Torrance, CA) and frozen in a dry-ice-isopentane bath and stored at −80 °C. For all other immunochemical and GFP fluorescence analysis, mice injected at a dose of 5×10^{11} vg/mouse were trans-cardially perfused at 4 weeks postinfusion with ice-cold 1× PBS. Retinas were removed prior to perfusion. Lungs were inflated in 0.5% low melting point agarose in 10% formalin-PBS solution postperfusion.

For biodistribution analysis, mice were trans-cardially perfused at 4 weeks postinfusion with ice-cold 1× PBS. Tissues were harvested immediately, frozen on dry ice, and stored at −80 °C.

Cat studies. AAV-B1 vector was packaged and purified as described earlier, and administered through the carotid artery into a 2-month-old normal domestic short haired cat at a dose of 3.4×10^{12} vg. At 4 weeks postinfusion, the injected cat was trans-cardially perfused with cold 1× PBS. Various tissues were harvested and fixed in 4% paraformaldehyde solution at 4 °C. The brain was cut into 0.6 cm coronal blocks prior to immersion in fixative. Processing of postfixed brains and spinal cords for IHC studies was identical to that for mouse studies. For GFP immunofluorescence studies, 30 µm sections of liver, skeletal, and cardiac muscle were incubated for 24 hours in rabbit polyclonal anti-GFP (1:1,000, Life Technologies, A11122) at 4 °C. After washing in 1× PBS, sections were incubated for 1 hour at room temperature in appropriate secondary antibodies, washed in 1× PBS and mounted using Permafluor mounting media (Thermo Scientific).

Immunohistochemical detection of GFP expression. For chromogenic IHC, 40 µm serial sections of brains and 30 µm serial sections of spinal cord were incubated for 96 hours in anti-GFP primary antibody (ABfinity rabbit monoclonal anti-GFP 1:1,000, G10362, Life Technologies, Grand Island, NY) at 4 °C. After washing with 1× PBS, sections were incubated in appropriate biotinylated secondary antibody (biotinylated anti-rabbit antibody, Vector Laboratories, Burlingame, CA), followed by incubation in ABC reagent (PK-6100, Vector Laboratories). Sections were developed with 3,3′-diaminobenzidine reagent according to the manufacturer's instructions (SK-4100, Vector Laboratories), dehydrated with increasing concentrations of ethanol, cleared with xylene and mounted using Permount mounting medium (Fisher Scientific).

For immunofluorescence studies, 40 µm sections of brains and 30 µm sections of spinal cord were incubated for 24 hours in a cocktail of appropriate primary antibodies at 4 °C. The primary antibodies used were: rabbit polyclonal anti-GFP (1:1,000, Life Technologies, A11122), chicken polyclonal anti-GFP (1:2,000, Abcam, Cambridge, MA, ab13970), mouse monoclonal anti-NeuN (1:500, EMD Millipore, Billerica, MA, MAB377), mouse monoclonal anti-DARPP32 (1:250, BD Biosciences, Franklin Lakes, NJ, 611520), mouse monoclonal anti-tyrosine hydroxylase (1:100, EMD Millipore, MAB318), mouse monoclonal anti-calbindin-D-28K (1:500, Sigma, St. Louis, MO, C9848), mouse monoclonal anti-APC (1:1,000, EMD Millipore, OP80) and rabbit polyclonal anti-CD31 (1:50, Abcam, ab28364). After washing in 1× PBS, sections were incubated for 1 hour at room temperature in appropriate secondary antibodies, washed in 1× PBS and mounted using Permafluor mounting media (Thermo Scientific). Native GFP fluorescence in liver and muscle groups was analyzed in 30 µm formalin-fixed sections, and 10 µm frozen sections, respectively. 7 µm formalin fixed pancreatic sections were analyzed with the following primary antibodies: rabbit polyclonal anti-GFP (1:1,000, Life Technologies, A11122), and guinea pig polyclonal anti-insulin (1:200, Abcam, ab7842). GFP expression in 10 µm formalin fixed lung sections was detected by chromogenic IHC after 24 hours incubation with rabbit polyclonal anti-GFP antibody (1:1,000, Life Technologies, A11122). Retinas were immunochemically processed as previously described (Punzo 2009), using rabbit polyclonal anti-GFP (1:1,000, Life Technologies, A11122). All images were captured on a Leica DM5500 B microscope (Leica Microsystems, Buffalo Grove, IL), except the muscle groups, which were imaged on a Zeiss microscope with Axiocam system. Postprocessing of images was performed using Adobe Photoshop CS6 (Adobe Systems, San Jose, CA).

Quantification of GFP-positive neurons in motor cortex, striatum, and thalamus. Chromogenic IHC staining of 40 µm mouse brain sections was performed as described in an earlier section. Four 663.28 × 497.40 µm regions were randomly chosen from the motor cortex, striatum or thalamus ($n = 4$ biological replicates per vector) of the stained sections. Neurons were identified by their morphology and manually counted. Motor neurons in thoracic spinal cord sections were additionally identified by their location (in laminae VIII and IX). All statistical analyses were performed using GraphPad Prism (GraphPad Software, La Jolla, CA). Total neurons in the 663.28 × 497.40 µm fields were counted in Nissl (cresyl violet acetate) stained brain sections using ImageJ software (National Institutes of Health, Bethesda, MD). Significance was determined by Student's unpaired two-tailed *T*-test. A $P < 0.05$ was considered to be significant.

Biodistribution analysis. Vector genome copy numbers from various mouse tissues were determined by qPCR after extraction of total DNA using DNeasy Blood and Tissue kit (Qiagen). Tissues were mechanically lysed using TissueLyzer II (Qiagen). Vector genome content in each tissue was determined using 100 ng total DNA using the same qPCR method described above for AAV vector titration. All statistical analyses were performed using GraphPad Prism (GraphPad Software). Significance was determined by Student's unpaired *T*-test. A $P < 0.05$ was considered to be significant.

Western blotting to assess GFP protein levels in various tissues was performed as follows. Total protein for western blotting was isolated from harvested tissues by bead lysis in T-PER tissue extraction reagent (Life Technologies) and quantified by Bradford assay. Total protein (20 µg) was separated by polyacrylamide gel electrophoresis using 4–20% Mini-PROTEAN TGX gels (Bio-Rad Laboratories, Hercules, CA) followed by transfer to nitrocellulose membranes and detection using primary antibodies for GFP (chicken polyclonal anti-GFP, 1:2,000, Aves Labs, Tigard, OR, GFP-1010) and mouse β-actin (mouse monoclonal anti-β-actin, 1:1,000, Sigma-Aldrich, A5441). Detection was done using appropriate IRDye secondary antibodies (LI-COR, Lincoln, NE). Tissues from four mice per group were used for analysis. Detection and quantification were done with Odyssey infrared imaging system (LI-COR).

Structural analysis. Alignment of AAV-B1 capsid protein sequence with parental serotypes was carried out using Cobalt Constraint-based Multiple Protein Alignment Tool.

The capsid sequence ordering was arranged using Chimera (http://www.cgl.ucsf.edu/chimera) in descending percent identities referenced to AAV8. The 3D model of AAV-B1 was generated using SWISS MODEL subroutine[63] based on coordinates from the AAV8 crystal structure[64] (PDB accession no. 2QA0) as a template. Surface mapping was performed using Pymol (http://www.pymol.org).

Antibody neutralization assay. Anti-AAV neutralization assay was performed as previously described.[65] Briefly, AAV vectors were mixed with varying concentrations of Gammagard S/D purified intravenous immunoglobulin (IVIg), (Baxter, Deerfield, IL, gift from Dr. Luk H. Vandenberghe, Harvard Medical School, MA) in serum-free media, incubated for 1 hour at 37 °C and then added to HeLa cells at 3.5×10^4 v.g./cell at 37 °C. AAV incubated with PBS (no IVIg) served as control. Ninety minutes later, cells were washed thrice with cold serum-free media and replacing with complete media, cells were incubated for 48 hours prior to trypsinization and preparation for flow cytometry. Cell samples were analyzed for GFP expression using the blue laser of a BD LSR Fortessa flow cytometer (San Jose, CA) running BD FACSDiva software (v6.1.3). Flow data were analyzed using FLOWJo software (FLOWJo, LLC, Ashland, OR). To calculate % transduction of control for the samples mixed with IVIg, we calculated fluorescence index (FI), for each sample. FI was calculated by multiplying the % GFP-positive cell values with the mean fluorescence intensity for each sample. We then divided the FI of the samples in the presence of IVIg to the FI of the samples in the control media to calculate % transduction of control.

In vitro *binding assay.* Pro5 and Lec2 CHO cell lines were gifts from Dr. Aravind Asokan (University of North Carolina, Chapel Hill, NC) and binding assay was performed as previously described.[29] Briefly, cells were prechilled for 30 minutes at 4 °C in serum-free Dulbecco's Modified Eagle

Medium (DMEM) (Life Technologies), followed by incubation with AAV vectors at 1×10^2, 5×10^2, 1×10^3, 5×10^3, 1×10^4, and 5×10^4 vg/cell in cold serum-free DMEM at 4 °C. Ninety minutes later, cells were washed thrice with cold serum-free DMEM to remove loosely bound vector particles. Cells incubated with vehicle (1× PBS in cold serum-free DMEM) were used as controls (0 vg/cell). Cells were harvested and total DNA was extracted using DNeasy Blood and Tissue kit (Qiagen). Vector genome copy numbers of cell surface bound virions was quantified by qPCR as described earlier. Binding curves were generated using GraphPad Prism software by fitting the single-site binding model, as described in a previous report.[29]

SUPPLEMENTARY MATERIAL

Figure S1. Chimeric nature of packaged viral library.
Figure S2. Transduction profile of AAV-B1 and AAV9 vector across multiple CNS regions after systemic delivery.
Figure S3. Phenotype of GFP positive cells in CNS after systemic delivery of AAV-B1.
Figure S4. Comparison of AAV-B1 capsid protein sequence to AAV8 and other natural AAV isolates.
Figure S5. Biodistribution profile of AAV-B1 and AAV8 vectors infused systemically at 5x1011 vg.
Figure S6. Antibody resistance assay comparing AAV9 and AAVB1.

ACKNOWLEDGMENTS

We thank Damien J. Cabral and Yves T. Falanga for technical assistance, and Guangping Gao, Erica Mondo, and Christian Mueller for technical advice. This work was supported by grant R01NS066310 (M.S.-E.). R.M.K. is an employee of Voyager Therapeutics and holds equity in the company.

REFERENCES

1. Bryant, LM, Christopher, DM, Giles, AR, Hinderer, C, Rodriguez, JL, Smith, JB *et al.* (2013). Lessons learned from the clinical development and market authorization of Glybera. *Hum Gene Ther Clin Dev* **24**: 55–64.
2. Cideciyan, AV, Hauswirth, WW, Aleman, TS, Kaushal, S, Schwartz, SB, Boye, SL *et al.* (2009). Vision 1 year after gene therapy for Leber's congenital amaurosis. *N Engl J Med* **361**: 725–727.
3. Nathwani, AC, Tuddenham, EG, Rangarajan, S, Rosales, C, McIntosh, J, Linch, DC *et al.* (2011). Adenovirus-associated virus vector-mediated gene transfer in hemophilia B. *N Engl J Med* **365**: 2357–2365.
4. Gaudet, D, Méthot, J, Déry, S, Brisson, D, Essiembre, C, Tremblay, G *et al.* (2013). Efficacy and long-term safety of alipogene tiparvovec (AAV1-LPLS447X) gene therapy for lipoprotein lipase deficiency: an open-label trial. *Gene Ther* **20**: 361–369.
5. Muramatsu, S, Fujimoto, K, Kato, S, Mizukami, H, Asari, S, Ikeguchi, K *et al.* (2010). A phase I study of aromatic L-amino acid decarboxylase gene therapy for Parkinson's disease. *Mol Ther* **18**: 1731–1735.
6. Hwu, WL, Muramatsu, S, Tseng, SH, Tzen, KY, Lee, NC, Chien, YH *et al.* (2012). Gene therapy for aromatic L-amino acid decarboxylase deficiency. *Sci Transl Med* **4**: 134ra61.
7. Leone, P, Shera, D, McPhee, SW, Francis, JS, Kolodny, EH, Bilaniuk, LT *et al.* (2012). Long-term follow-up after gene therapy for canavan disease. *Sci Transl Med* **4**: 165ra163.
8. Worgall, S, Sondhi, D, Hackett, NR, Kosofsky, B, Kekatpure, MV, Neyzi, N *et al.* (2008). Treatment of late infantile neuronal ceroid lipofuscinosis by CNS administration of a serotype 2 adeno-associated virus expressing CLN2 cDNA. *Hum Gene Ther* **19**: 463–474.
9. Tardieu, M, Zérah, M, Husson, B, de Bournonville, S, Deiva, K, Adamsbaum, C *et al.* (2014). Intracerebral administration of adeno-associated viral vector serotype rh.10 carrying human SGSH and SUMF1 cDNAs in children with mucopolysaccharidosis type IIIA disease: results of a phase I/II trial. *Hum Gene Ther* **25**: 506–516.
10. Eberling, JL, Jagust, WJ, Christine, CW, Starr, P, Larson, P, Bankiewicz, KS *et al.* (2008). Results from a phase I safety trial of hAADC gene therapy for Parkinson disease. *Neurology* **70**: 1980–1983.
11. Zhang, H, Yang, B, Mu, X, Ahmed, SS, Su, Q, He, R *et al.* (2011). Several rAAV vectors efficiently cross the blood-brain barrier and transduce neurons and astrocytes in the neonatal mouse central nervous system. *Mol Ther* **19**: 1440–1448.
12. Foust, KD, Nurre, E, Montgomery, CL, Hernandez, A, Chan, CM and Kaspar, BK (2009). Intravascular AAV9 preferentially targets neonatal neurons and adult astrocytes. *Nat Biotechnol* **27**: 59–65.
13. Foust, KD, Wang, X, McGovern, VL, Braun, L, Bevan, AK, Haidet, AM *et al.* (2010). Rescue of the spinal muscular atrophy phenotype in a mouse model by early postnatal delivery of SMN. *Nat Biotechnol* **28**: 271–274.
14. Foust, KD, Salazar, DL, Likhite, S, Ferraiuolo, L, Ditsworth, D, Ilieva, H *et al.* (2013). Therapeutic AAV9-mediated suppression of mutant SOD1 slows disease progression and extends survival in models of inherited ALS. *Mol Ther* **21**: 2148–2159.
15. Fu, H, Dirosario, J, Killedar, S, Zaraspe, K and McCarty, DM (2011). Correction of neurological disease of mucopolysaccharidosis IIIB in adult mice by rAAV9 trans-blood-brain barrier gene delivery. *Mol Ther* **19**: 1025–1033.
16. Ruzo, A, Marcó, S, García, M, Villacampa, P, Ribera, A, Ayuso, E *et al.* (2012). Correction of pathological accumulation of glycosaminoglycans in central nervous system and peripheral tissues of MPSIIIA mice through systemic AAV9 gene transfer. *Hum Gene Ther* **23**: 1237–1246.
17. Ahmed, SS, Li, H, Cao, C, Sikoglu, EM, Denninger, AR, Su, Q *et al.* (2013). A single intravenous rAAV injection as late as P20 achieves efficacious and sustained CNS Gene therapy in Canavan mice. *Mol Ther* **21**: 2136–2147.
18. Garg, SK, Lioy, DT, Cheval, H, McGann, JC, Bissonnette, JM, Murtha, MJ *et al.* (2013). Systemic delivery of MeCP2 rescues behavioral and cellular deficits in female mouse models of Rett syndrome. *J Neurosci* **33**: 13612–13620.
19. Weismann, CM, Ferreira, J, Keeler, AM, Su, Q, Qui, L, Shaffer, SA *et al.* (2015). Systemic AAV9 gene transfer in adult GM1 gangliosidosis mice reduces lysosomal storage in CNS and extends lifespan. *Hum Mol Genet* **24**: 4353–4364.
20. Yang, B, Li, S, Wang, H, Guo, Y, Gessler, DJ, Cao, C *et al.* (2014). Global CNS transduction of adult mice by intravenously delivered rAAVrh.8 and rAAVrh.10 and nonhuman primates by rAAVrh.10. *Mol Ther* **22**: 1299–1309.
21. Duque, S, Joussemet, B, Riviere, C, Marais, T, Dubreil, L, Douar, AM *et al.* (2009). Intravenous administration of self-complementary AAV9 enables transgene delivery to adult motor neurons. *Mol Ther* **17**: 1187–1196.
22. Bevan, AK, Duque, S, Foust, KD, Morales, PR, Braun, L, Schmelzer, L *et al.* (2011). Systemic gene delivery in large species for targeting spinal cord, brain, and peripheral tissues for pediatric disorders. *Mol Ther* **19**: 1971–1980.
23. Gombash, SE, Cowley, CJ, Fitzgerald, JA, Hall, JC, Mueller, C, Christofi, FL *et al.* (2014). Intravenous AAV9 efficiently transduces myenteric neurons in neonate and juvenile mice. *Front Mol Neurosci* **7**: 81.
24. Benskey, MJ, Kuhn, NC, Galligan, JJ, Garcia, J, Boye, SE, Hauswirth, WW *et al.* (2015). Targeted gene delivery to the enteric nervous system using AAV: a comparison across serotypes and capsid mutants. *Mol Ther* **23**: 488–500.
25. DiMattia, MA, Nam, HJ, Van Vliet, K, Mitchell, M, Bennett, A, Gurda, BL *et al.* (2012). Structural insight into the unique properties of adeno-associated virus serotype 9. *J Virol* **86**: 6947–6958.
26. Xie, Q, Bu, W, Bhatia, S, Hare, J, Somasundaram, T, Azzi, A *et al.* (2002). The atomic structure of adeno-associated virus (AAV-2), a vector for human gene therapy. *Proc Natl Acad Sci USA* **99**: 10405–10410.
27. Wu, Z, Miller, E, Agbandje-McKenna, M and Samulski, RJ (2006). Alpha2,3 and alpha2,6 N-linked sialic acids facilitate efficient binding and transduction by adeno-associated virus types 1 and 6. *J Virol* **80**: 9093–9103.
28. Kaludov, N, Brown, KE, Walters, RW, Zabner, J and Chiorini, JA (2001). Adeno-associated virus serotype 4 (AAV4) and AAV5 both require sialic acid binding for hemagglutination and efficient transduction but differ in sialic acid linkage specificity. *J Virol* **75**: 6884–6893.
29. Shen, S, Bryant, KD, Brown, SM, Randell, SH and Asokan, A (2011). Terminal N-linked galactose is the primary receptor for adeno-associated virus 9. *J Biol Chem* **286**: 13532–13540.
30. Bell, CL, Vandenberghe, LH, Bell, P, Limberis, MP, Gao, GP, Van Vliet, K *et al.* (2011). The AAV9 receptor and its modification to improve *in vivo* lung gene transfer in mice. *J Clin Invest* **121**: 2427–2435.
31. Gao, GP, Alvira, MR, Wang, L, Calcedo, R, Johnston, J and Wilson, JM (2002). Novel adeno-associated viruses from rhesus monkeys as vectors for human gene therapy. *Proc Natl Acad Sci USA* **99**: 11854–11859.
32. Gao, G, Alvira, MR, Somanathan, S, Lu, Y, Vandenberghe, LH, Rux, JJ *et al.* (2003). Adeno-associated viruses undergo substantial evolution in primates during natural infections. *Proc Natl Acad Sci USA* **100**: 6081–6086.
33. Gao, G, Vandenberghe, LH, Alvira, MR, Lu, Y, Calcedo, R, Zhou, X *et al.* (2004). Clades of Adeno-associated viruses are widely disseminated in human tissues. *J Virol* **78**: 6381–6388.
34. Bartel, MA, Weinstein, JR and Schaffer, DV (2012). Directed evolution of novel adeno-associated viruses for therapeutic gene delivery. *Gene Ther* **19**: 694–700.
35. Maheshri, N, Koerber, JT, Kaspar, BK and Schaffer, DV (2006). Directed evolution of adeno-associated virus yields enhanced gene delivery vectors. *Nat Biotechnol* **24**: 198–204.
36. Excoffon, KJ, Koerber, JT, Dickey, DD, Murtha, M, Keshavjee, S, Kaspar, BK *et al.* (2009). Directed evolution of adeno-associated virus to an infectious respiratory virus. *Proc Natl Acad Sci USA* **106**: 3865–3870.
37. Grimm, D, Lee, JS, Wang, L, Desai, T, Akache, B, Storm, TA *et al.* (2008). *In vitro* and *in vivo* gene therapy vector evolution via multispecies interbreeding and retargeting of adeno-associated viruses. *J Virol* **82**: 5887–5911.
38. Yang, L, Jiang, J, Drouin, LM, Agbandje-McKenna, M, Chen, C, Qiao, C *et al.* (2009). A myocardium tropic adeno-associated virus (AAV) evolved by DNA shuffling and in vivo selection. *Proc Natl Acad Sci USA* 106: 3946–3951.
39. Gray, SJ, Blake, BL, Criswell, HE, Nicolson, SC, Samulski, RJ, McCown, TJ *et al.* (2010). Directed evolution of a novel adeno-associated virus (AAV) vector that crosses the seizure-compromised blood-brain barrier (BBB). *Mol Ther* **18**: 570–578.
40. Dalkara, D, Byrne, LC, Klimczak, RR, Visel, M, Yin, L, Merigan, WH *et al.* (2013). In vivo-directed evolution of a new adeno-associated virus for therapeutic outer retinal gene delivery from the vitreous. *Sci Transl Med* **5**: 189ra76.
41. Lisowski, L, Dane, AP, Chu, K, Zhang, Y, Cunningham, SC, Wilson, EM *et al.* (2014). Selection and evaluation of clinically relevant AAV variants in a xenograft liver model. *Nature* **506**: 382–386.
42. Choudhury, SR, Harris, AF, Cabral, DJ, Keeler, AM, Sapp, E, Ferreira, JS *et al.* (2016). Widespread central nervous system gene transfer and silencing after systemic delivery of novel AAV-AS vector. *Mol Ther* **24**: 726–735.
43. Deverman, BE, Pravdo, PL, Simpson, BP, Kumar, SR, Chan, KY, Banerjee, A *et al.* (2016). Cre-dependent selection yields AAV variants for widespread gene transfer to the adult brain. *Nat Biotechnol* **34**: 204–209.
44. Gray, SJ, Matagne, V, Bachaboina, L, Yadav, S, Ojeda, SR and Samulski, RJ (2011). Preclinical differences of intravascular AAV9 delivery to neurons and glia: a comparative study of adult mice and nonhuman primates. *Mol Ther* **19**: 1058–1069.

45. Bemelmans, AP, Duqué, S, Rivière, C, Astord, S, Desrosiers, M, Marais, T *et al.* (2013). A single intravenous AAV9 injection mediates bilateral gene transfer to the adult mouse retina. *PLoS One* **8**: e61618.
46. McCurdy, VJ, Johnson, AK, Gray-Edwards, HL, Randle, AN, Brunson, BL, Morrison, NE *et al.* (2014). Sustained normalization of neurological disease after intracranial gene therapy in a feline model. *Sci Transl Med* **6**: 231ra48.
47. Bradbury, AM, Cochran, JN, McCurdy, VJ, Johnson, AK, Brunson, BL, Gray-Edwards, H *et al.* (2013). Therapeutic response in feline sandhoff disease despite immunity to intracranial gene therapy. *Mol Ther* **21**: 1306–1315.
48. Yoon, SY, Bagel, JH, O'Donnell, PA, Vite, CH and Wolfe, JH (2016). Clinical improvement of alpha-mannosidosis cat following a single cisterna magna infusion of AAV1. *Mol Ther* **24**: 26–33.
49. Vite, CH, Bagel, JH, Swain, GP, Prociuk, M, Sikora, TU, Stein, VM *et al.* (2015). Intracisternal cyclodextrin prevents cerebellar dysfunction and Purkinje cell death in feline Niemann-Pick type C1 disease. *Sci Transl Med* **7**: 276ra26.
50. Manno, CS, Pierce, GF, Arruda, VR, Glader, B, Ragni, M, Rasko, JJ *et al.* (2006). Successful transduction of liver in hemophilia by AAV-Factor IX and limitations imposed by the host immune response. *Nat Med* **12**: 342–347.
51. Bankiewicz, KS, Eberling, JL, Kohutnicka, M, Jagust, W, Pivirotto, P, Bringas, J *et al.* (2000). Convection-enhanced delivery of AAV vector in parkinsonian monkeys; *in vivo* detection of gene expression and restoration of dopaminergic function using pro-drug approach. *Exp Neurol* **164**: 2–14.
52. Cearley, CN and Wolfe, JH (2007). A single injection of an adeno-associated virus vector into nuclei with divergent connections results in widespread vector distribution in the brain and global correction of a neurogenetic disease. *J Neurosci* **27**: 9928–9940.
53. Kells, AP, Hadaczek, P, Yin, D, Bringas, J, Varenika, V, Forsayeth, J *et al.* (2009). Efficient gene therapy-based method for the delivery of therapeutics to primate cortex. *Proc Natl Acad Sci USA* **106**: 2407–2411.
54. Salegio, EA, Samaranch, L, Kells, AP, Mittermeyer, G, San Sebastian, W, Zhou, S *et al.* (2013). Axonal transport of adeno-associated viral vectors is serotype-dependent. *Gene Ther* **20**: 348–352.
55. San Sebastian, W, Samaranch, L, Heller, G, Kells, AP, Bringas, J, Pivirotto, P *et al.* (2013). Adeno-associated virus type 6 is retrogradely transported in the non-human primate brain. *Gene Ther* **20**: 1178–1183.
56. DeRuisseau, LR, Fuller, DD, Qiu, K, DeRuisseau, KC, Donnelly, WH Jr, Mah, C *et al.* (2009). Neural deficits contribute to respiratory insufficiency in Pompe disease. *Proc Natl Acad Sci USA* **106**: 9419–9424.
57. Falk, DJ, Soustek, MS, Todd, AG, Mah, CS, Cloutier, DA, Kelley, JS *et al.* (2015). Comparative impact of AAV and enzyme replacement therapy on respiratory and cardiac function in adult Pompe mice. *Mol Ther Methods Clin Dev* **2**: 15007.
58. Cardone, M, Porto, C, Tarallo, A, Vicinanza, M, Rossi, B, Polishchuk, E *et al.* (2008). Abnormal mannose-6-phosphate receptor trafficking impairs recombinant alpha-glucosidase uptake in Pompe disease fibroblasts. *Pathogenetics* **1**: 6.
59. Pillay, S, Meyer, NL, Puschnik, AS, Davulcu, O, Diep, J, Ishikawa, Y *et al.* (2016). An essential receptor for adeno-associated virus infection. *Nature* **530**: 108–112.
60. Allay, JA, Sleep, S, Long, S, Tillman, DM, Clark, R, Carney, G *et al.* (2011). Good manufacturing practice production of self-complementary serotype 8 adeno-associated viral vector for a hemophilia B clinical trial. *Hum Gene Ther* **22**: 595–604.
61. Li, W, Asokan, A, Wu, Z, Van Dyke, T, DiPrimio, N, Johnson, JS *et al.* (2008). Engineering and selection of shuffled AAV genomes: a new strategy for producing targeted biological nanoparticles. *Mol Ther* **16**: 1252–1260.
62. Zolotukhin, S, Byrne, BJ, Mason, E, Zolotukhin, I, Potter, M, Chesnut, K *et al.* (1999). Recombinant adeno-associated virus purification using novel methods improves infectious titer and yield. *Gene Ther* **6**: 973–985.
63. Biasini, M, Bienert, S, Waterhouse, A, Arnold, K, Studer, G, Schmidt, T *et al.* (2014). SWISS-MODEL: modelling protein tertiary and quaternary structure using evolutionary information. *Nucleic Acids Res* **42**(Web Server issue): W252–W258.
64. Nam, HJ, Lane, MD, Padron, E, Gurda, B, McKenna, R, Kohlbrenner, E *et al.* (2007). Structure of adeno-associated virus serotype 8, a gene therapy vector. *J Virol* **81**: 12260–12271.
65. György, B, Fitzpatrick, Z, Crommentuijn, MH, Mu, D and Maguire, CA (2014). Naturally enveloped AAV vectors for shielding neutralizing antibodies and robust gene delivery in vivo. *Biomaterials* **35**: 7598–7609.